THE ASTROPHYSICAL JOURNAL, 352:139–148, 1990 March 20

MOLECULAR OUTFLOWS ASSOCIATED WITH A FLUX-LIMITED SAMPLE OF BRIGHT FAR-INFRARED SOURCES

RONALD L. SNELL, ROBERT L. DICKMAN, AND Y.-L. HUANG
Five College Radio Astronomy Observatory; and Department of Physics and Astronomy, University of Massachusetts
Received 1989 June; accepted 1989 September 12

ABSTRACT

We report the results of a systematic search for high-velocity CO emission from a sample of bright (100 μm flux densities >500 Jy) far-infrared sources from the *IRAS* Point Source Catalog. This extends our original survey to a complete flux-limited sample. In this paper we present results of CO mapping toward 22 far-infrared sources and find all to be associated with strong CO emission that is peaked close to the far-infrared sources. Based on their infrared colors and positional coincidence with strong CO emission, we believe our sample to be composed entirely of luminous, young stellar objects. New detections of molecular outflows were made toward six of the far-infrared sources; these outflows are relatively energetic, with typical mechanical energies of 10^{45} ergs. Combining our two surveys and including other published results, we find that roughly 50% of a flux-limited sample of far-infrared sources have energetic molecular outflows. The short lifetime of the outflow phase coupled with the high incidence of outflows is used to set an upper limit of 4×10^5 yr for the lifetime of stars as luminous far-infrared sources. Outflows may make an important contribution to the kinetic energy density within molecular clouds.

Subject headings: infrared: sources — interstellar: molecules — nebulae: internal motions — stars: formation

I. INTRODUCTION

Energetic and often highly collimated stellar winds are a well-established aspect of the evolution of young stellar objects (YSOs). Observations of the ambient molecular gas accelerated by these stellar winds are a powerful means to study this energetic phenomenon, since the optical and near-infrared light emitted by stellar winds is usually obscured from view. Further, the large energy and momentum content of many molecular outflows implies the existence of massive, driving stellar winds which must have a profound effect on surrounding circumstellar material and on the future development of star formation in clouds that they occupy. For this reason, the frequency of the outflow phenomenon, the nature of the objects responsible for it, and the energies involved, are all essential parameters for understanding the star formation process. In a recent paper (Snell *et al.* 1988, hereafter Paper I) we presented results of a search for molecular outflows in a sample of bright far-infrared sources found by the *Infrared Astronomical Satellite* (*IRAS*). The use of the *IRAS* survey data has now allowed for a more systematic search for outflows from YSOs and has permitted a more definitive determination of the frequency of energetic outflows. In this paper we thus extend our original survey to a complete flux-limited sample of sources at 100 μm.

In Paper I we chose a sample of bright far-infrared (FIR) sources from the *IRAS* Point Source Catalog (1985) based solely on their infrared properties. Our selection criteria in Paper I were the following: (1) the sources were required to have $S(100\ \mu\text{m}) > 500$ Jy; (2) their right ascension had to lie between R.A. 0^h and 12^h; (3) their declination had to be greater than 0°; and (4) the sources had to be detected at all four *IRAS* wavelengths and in the earlier Air Force Geophysics Laboratory (AFGL) surveys (Price and Walker 1976; Price 1977). The first criterion was imposed to restrict the sample to a manageable size. The second criterion was imposed to avoid lines of sight through the inner Galaxy, where it is difficult to separate Galactic emission from high-velocity outflows. The third criterion simply ensured that the sources transited at high elevations at the Five College Radio Astronomy Observatory (FCRAO). The last criterion was designed to ensure that the sample consisted of decisively stellar objects. Unfortunately, this last criterion also had the effect of eliminating the reddest YSOs in the *IRAS* catalog, since these were often not detected at the shorter infrared wavelengths of the AFGL and *IRAS* surveys.

We have now extended our original survey to contain all sources in the right ascension and declination range given above with $S(100\ \mu\text{m}) > 500$ Jy, and we will show that these objects are almost certainly all young stellar objects. The number of sources meeting these criteria is 51 (excluding IRC +10216 and M82), of which 12 were previously listed as outflow sources (Lada 1985). Of the 39 remaining sources, we surveyed 18 in Paper I, and in this paper we present the results of observations of the remaining 21 sources. We also have mapped the region around S235B, a source in the outflow catalog of Lada (1985) but one for which no mapping data have been previously published.

II. OBSERVATIONS AND RESULTS

The observations of the $J = 1$–0 transition of ^{12}CO were obtained with the 14 m telescope of the Five College Radio Astronomy Observatory in New Salem, Massachusetts.[1] The data calibration and spectrometer setup were the same as those described in Paper I. Temperatures quoted in this paper are in units of T_R^*, i.e., antenna temperature corrected for atmospheric, spillover, and scattering losses from the antenna and radome. An additional correction has been applied in calculation of the outflow energetics to account for the beam cou-

[1] The Five College Radio Astronomy Observatory is operated with support from the National Science Foundation (grant AST 85-12903) and the Commonwealth of Massachusetts with permission of the Metropolitan District Commission.

pling efficiency, estimated to be 0.7 for the high-velocity outflows.

We began our survey by obtaining small 3 × 3 point maps, spaced by either 1′ or 1.′5, centered on each of the 22 *IRAS* point sources. As pointed out in Paper I, this search strategy reduced the chance of missing outflows, since outflow emission is often extended and separated from the driving stellar source. The rms noise in the 0.25 MHz (0.65 km s^{-1}) resolution filter bank was typically 0.20 K. The positions of the 22 *IRAS* point sources observed are given in Table 1. In all cases except 05375+3540 (S235B), the maps were either filled in at finer spacings or extended for better definition of the nature and extent of the molecular emission. The number of points in each map is given in Table 1.

CO emission was detected toward all 22 *IRAS* point sources; a summary of the emission seen toward each source is presented in Table 1. Except for 04073+5102, emission greater than a few kelvins was detected at only one velocity in each source. In 04073+5102 relatively strong velocity components at $V_{LSR} = -53$, -49, -37, and -26 km s^{-1} were detected. The two strongest components were those at -53 and -49 km s^{-1}, and the component at -53 km s^{-1} was peaked toward the *IRAS* source; we thus associate the -53 km s^{-1} component with this source. (The -49 km s^{-1} feature likely arises from a cloud closely associated with the -53 km s^{-1} cloud, since the maximum in its CO emission lies only 2′ to the south-east.)

In general, the CO emission detected toward the sources we observed is quite strong, exceeding 10 K in 16 of the 22 sources. Maps of the peak antenna temperature around 21 of the *IRAS* sources are shown in Figure 1. (The map of 04073+5102 includes both the -49 and the -53 km s^{-1} components.) Only in 06380+0949 was the map obtained not extensive enough to locate a peak in the CO emission; the larger map of Margulis and Lada (1986) suggests that this source is associated with the Mon OB1 molecular cloud. In the other 21 sources the maximum CO emission lies close to the *IRAS* source, though in some cases (notably 02244+6117, 03953+5110, and 06013+3030) the *IRAS* source is displaced from the CO peak by as much as 2′. It is not certain whether these displacements are real or are caused in part by poor accuracy in the *IRAS* coordinates. Based on the positional coincidences between *IRAS* sources and CO emission peaks in this survey and that presented in Paper I, there is clearly good reason to believe that the CO emission arises from molecular gas associated with the *IRAS* sources. Likewise, the relative brightness of the detected CO emission suggests that the *IRAS* sources are providing the local gas heating needed to produce the strong CO emission.

While these are obviously strong *a priori* reasons for believing that the sources in our sample are YSOs, this hypothesis can be tested by examining the colors of the IR sources. From flux densities at 25, 60, and 100 μm given in the *IRAS* Point Source Catalog, we have computed $S(100\ \mu m)/S(60\ \mu m)$ and the $S(60\ \mu m)/S(25\ \mu m)$ colors. A color-color diagram for the sources in our sample is shown in Figure 2 (a few of the objects are not plotted because the flux at one of the three bands was tabulated as "confused" or as a limit in the Point Source Catalog). The two colors are correlated, with the reddest objects in (100 μm/60 μm) color also being the reddest in (60 μm/25 μm) color. All the sources in our sample have very similar colors, which are similar to the distinctive colors that massive stars embedded in molecular clouds have (Wood and Churchwell 1989). Thus, the close association of our sources with strong CO emission, as well as their far-infrared colors, suggests that these objects are YSOs still deeply embedded in the clouds from which they formed.

To estimate the total infrared luminosity of the sources, we need an estimate of the distance of each object in our survey. To estimate this quantity, we used a technique similar to that described in Paper I, in which we attempted to associate each source in position and velocity with H II regions and OB associations of known distances. Our estimates are summarized in Table 2, along with references to the distances of the associated H II regions and OB associations. Many of the sources in this sample and in the sample in Paper I lie between

TABLE 1

SUMMARY OF CO OBSERVATIONS

IRAS Name	Associated Sources	α(1950)	δ(1950)	T_R^* (K)	V_{LSR} (km s^{-1})	ΔV (km s^{-1})	Points
00338+6312.....	...	$00^h33^m53^s3$	+63°12′32″	13.2	−18.4	5.5	34
00494+5617.....	S184/NGC 281	00 49 27.8	+56 17 28	14.5	−30.5	6.2	25
02244+6117.....	AFGL 333	02 24 27.2	+61 17 47	15.6	−50.8	5.0	25
03595+5110.....	S206/AFGL 5111	03 59 31.6	+51 10 41	2.4	−23.3	2.3	22
04073+5102.....	S209/AFGL 550	04 07 18.5	+51 02 30	5.8	−53.2	3.9	26
04329+5047.....	S211/AFGL 5125	04 32 58.3	+50 47 21	8.7	−37.1	3.5	17
05197+3355.....	S230	05 19 46.4	+33 55 39	20.4	−4.0	2.7	25
05358+3543.....	S233	05 35 48.8	+35 43 41	17.0	−18.2	5.3	17
05375+3540.....	S235B	05 37 32.1	+35 40 45	20.9	−17.2	4.1	9
05377+3548.....	S235	05 37 46.7	+35 48 25	23.9	−20.0	4.5	17
05480+2544.....	BFS 48	05 48 01.9	+25 44 50	10.7	−9.3	4.2	17
05480+2545.....	BFS 48	05 48 04.8	+25 45 29	8.8	−9.0	4.5	17
05490+2658.....	S242	05 49 05.2	+26 58 52	15.5	+0.3	5.1	25
05553+1631.....	AFGL 5173	05 55 20.3	+16 31 46	17.6	+5.4	3.3	25
06006+3015.....	S241/AFGL 5176	06 00 41.4	+30 15 05	10.9	−7.8	6.4	17
06013+3030.....	...	06 01 21.2	+30 30 53	2.1	+2.7	3.3	17
06055+2039.....	S252A	06 05 33.9	+20 39 47	20.7	+8.1	5.0	17
06105+1756.....	S258	06 10 33.0	+17 56 22	11.5	+7.9	3.4	17
06117+1350.....	S269	06 11 46.4	+13 50 33	20.1	+18.5	4.0	17
06155+2319.....	BFS 51	06 15 32.7	+23 19 26	15.8	−6.2	3.0	25
06308+0402.....	RNO 73	06 30 52.7	+04 02 27	13.8	+15.4	3.8	17
06380+0949.....	S273/AFGL 4519	06 38 00.6	+09 49 24	5.1	+4.9	6.6	9

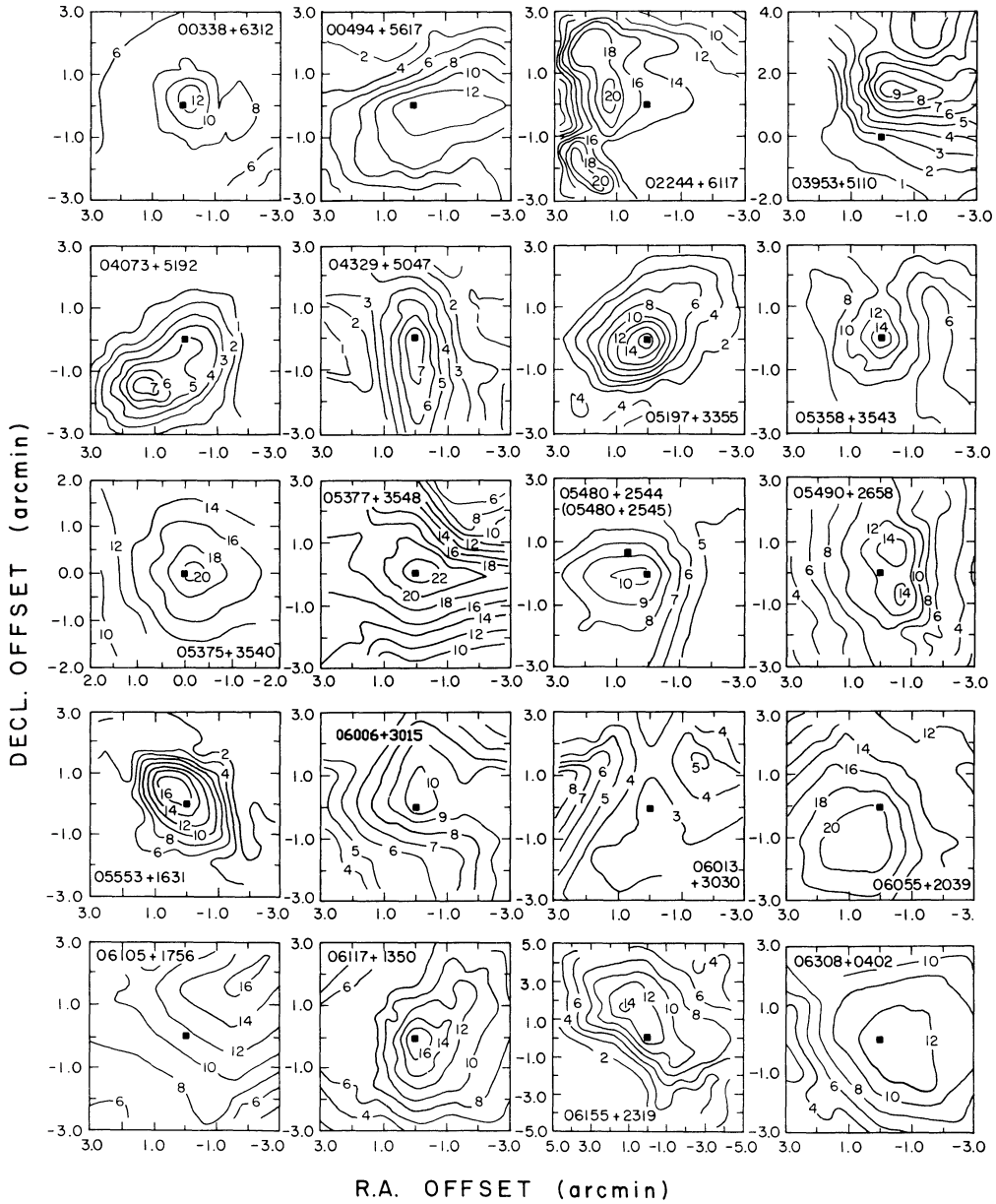

FIG. 1.—Maps of the peak ^{12}CO antenna temperature (T_R^*) around 21 of the far-infrared sources in our outflow survey. The locations of the far-infrared sources are marked by filled squares.

1.5 and 3.0 kpc from the Sun and in the vicinity of the Perseus arm of the Galaxy. Source luminosities have been estimated using the expression from Casoli *et al.* (1986) that gives an approximate far-infrared flux based on the flux densities in the Point Source Catalog at 12, 25, 60, and 100 μm. As was the case for the sources in Paper I,[2] the sources listed in Table 2 are all intrinsically luminous (luminosities range from 4×10^2 to 5×10^4 $L_\odot$), with an average luminosity of 2×10^4 $L_\odot$, a value consistent with their being recently formed O and B stars. A plot of far-infrared luminosity versus color is presented in Figure 3 and shows no evidence that the color and luminosity of objects in this sample are correlated.

[2] The luminosities published in Paper I were incorrectly computed and should all be multiplied by a factor of 0.54.

III. MOLECULAR OUTFLOWS

a) Survey

Based on our mapping data, we applied two criteria for identifying outflow activity. These are the following: (1) emission over a large velocity extent must be present, in general greater than 10 km s^{-1}, and (2) the high-velocity emission must be spatially confined to the region near the far-infrared source. Although care was taken to make maps sufficiently large to distinguish between superposed velocity components and true high-velocity molecular emission, and though the guidelines above were followed, in the end identifying outflows remains a somewhat subjective process.

In this work we have identified six new molecular outflows: 00338+6312, 00494+5617, 05358+3543, 05490+2658, 05553+1631, and 06308+0402. A summary of the properties

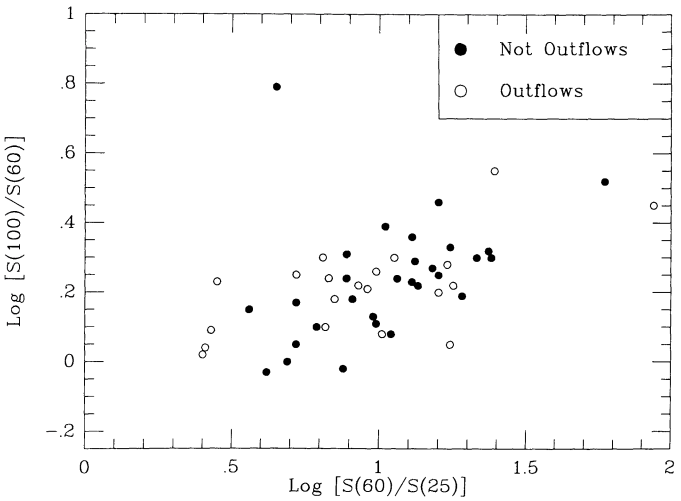

FIG. 2.—Two-color diagram for the bright far-infrared sources selected from the *IRAS* Point Source Catalog using flux densities at 25, 60, and 100 μm. The open circles are far-infrared sources associated with molecular outflows, and the filled circles are sources without detectable outflows.

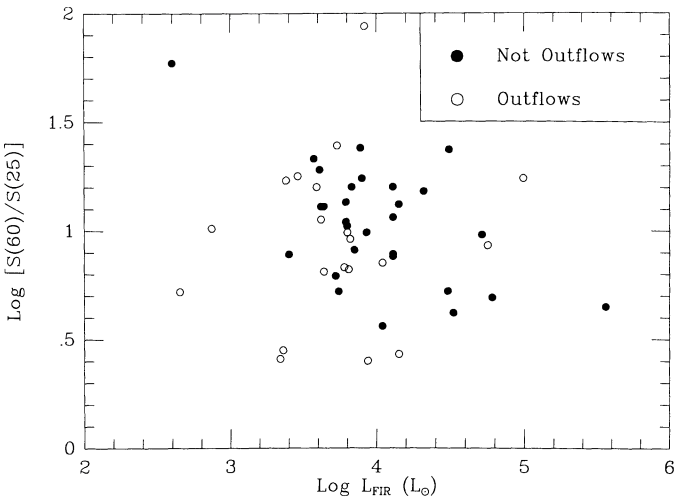

FIG. 3.—Plot of the color derived from the 25 and 60 μm flux densities vs. the far-infrared luminosity for the sources in our survey. Symbols are the same as Fig. 2.

of these outflows and the results of our mapping of 05375+3540 (S235B) are presented below.

i) *00338+6312*

Tentatively associated with Cas OB14, at a distance of 1.6 kpc (Humphreys 1978), 00338+6312 occurs at a velocity and position sparsely populated by molecular clouds. This source probably lies between the local " − 12 km s^{-1} " arm at a distance of 800 pc and the Perseus arm clouds (V_{LSR} = −45 km s^{-1}) at a distance of approximately 2.5 kpc (Cohen *et al.* 1980; Dame *et al.* 1987). ^{12}CO spectra obtained along a north-south line through this source are shown in Figure 4; a weak secondary velocity component is also present at −2 km s^{-1}. The high-velocity wings seen toward the source are quite prominent and symmetrical, and extend over a velocity range of 25 km s^{-1}. One-half arcminute south of the source the blue wing is more pronounced than the red wing, and 0.5 north of the source the red wing is more pronounced than the blue wing; farther north and south of the source the wings are not detectable at all. A map of the integrated intensity of the blue (−30 to −20 km s^{-1}) and red (−15 to −5 km s^{-1}) wings is shown in Figure 5 and shows clearly the bipolar nature of the outflow. The position of the far-infrared source is marked and lies close to the center of the outflow. The outflow has an extent of 2.5 (1.2 pc), much smaller than the extent of the molecular cloud seen in Figure 1.

TABLE 2

DISTANCES AND LUMINOSITIES OF *IRAS* SOURCES

IRAS Name	l	b	Distance (kpc)	Reference	L_{FIR} ($L_\odot$)
00338+6312.....	121°.3	+0°.7	1.6	1	2.4×10^3
00494+5617.....	123.1	−6.3	2.2	2	5.4×10^3
02244+6117.....	134.2	+0.8	2.2	3	7.8×10^3
03595+5110.....	150.6	−1.0	3.3	4	1.3×10^4
04073+5102.....	151.6	−0.2	12.1	5	3.6×10^5
04329+5047.....	154.6	+2.5	6.0	6	3.1×10^4
05197+3355.....	173.2	−1.3	3.2	7	7.9×10^3
05358+3543.....	173.5	+2.4	1.8	8	6.3×10^3
05375+3540.....	173.7	+2.7	1.8	8	1.3×10^4
05377+3548.....	173.6	+2.8	1.8	8	6.3×10^3
05480+2544.....	183.4	−0.6	2.1	9	3.5×10^3
05480+2545.....	183.4	−0.6	2.1	9	4.2×10^3
05490+2658.....	182.4	+0.3	2.1	9	4.2×10^3
05553+1631.....	192.2	−3.8	2.5	10	6.5×10^3
06006+3015.....	180.9	+4.1	4.7	11	1.3×10^4
06013+3030.....	180.7	+4.4	4.7	11	2.1×10^4
06055+2039.....	189.8	+0.3	1.5	12	6.0×10^3
06105+1756.....	192.7	+0.0	2.5	10	7.0×10^3
06117+1350.....	196.5	−1.7	3.8	13	5.1×10^4
06155+2319.....	188.6	+3.7	1.6	14	3.7×10^3
06308+0402.....	207.3	−2.2	1.6	15	3.9×10^3
06380+0949.....	203.0	+2.3	0.8	16	4.0×10^2

REFERENCES.—(1) Kinematic distance; (2) S184 (Georgelin and Georgelin 1976); (3) associated with Cas OB6 (Humphreys 1978); (4) near S206 (Moffat, FitzGerald, and Jackson 1979 [MFJ]; Crampton, Georgelin, and Georgelin 1978); (5) near S209 (Fich and Blitz 1984); (6) near S212 (MFJ); (7) near S236 (Blitz, Fich, and Stark 1982); (8) near S235 (Evans and Blair 1981); (9) near S242 (Y. Georgelin, quoted in Blitz, Fich, and Stark 1982); (10) near S255 (MFJ); (11) S241 (MFJ); (12) associated with Gem OB1 (Humphreys 1978); (13) S269 (MFJ); (14) near S249 (MFJ); (15) near S275 (Blitz and Thaddeus 1980); (16) S273 (Turner 1976).

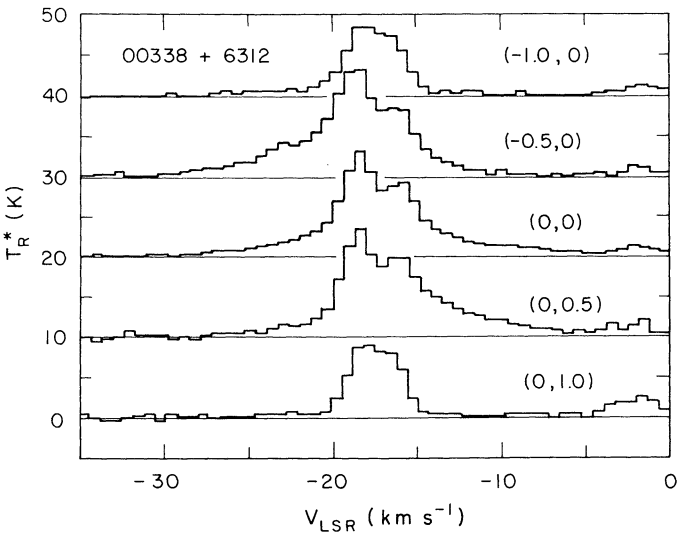

FIG. 4.—Spectra of the ^{12}CO line in the vicinity of 00338+6312. The location of each spectrum is given as an offset in arcminutes (R.A. offset, decl. offset) relative to the position of 00338+6312. From top to bottom, the spectra were obtained 1′ west, 0.5 west, toward, 0.5 north, and 1′ north of 00338+6312.

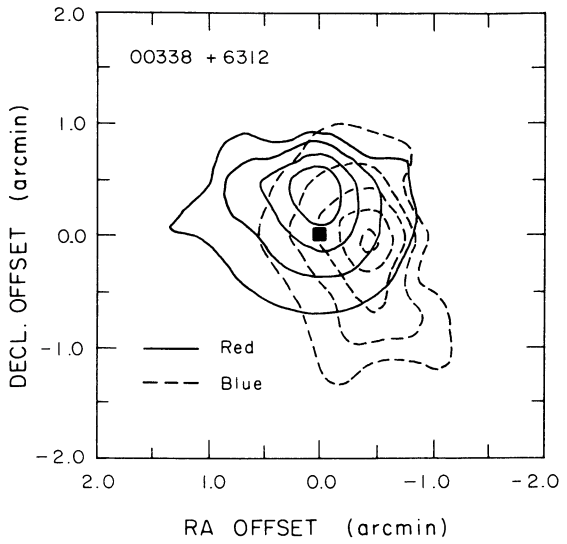

FIG. 5.—Maps of the integrated ^{12}CO intensity of the high-velocity redshifted (-15 to -5 km s^{-1}) and blueshifted (-30 to -20 km s^{-1}) emission near 00338+6312. The location of 00338+6312 is indicated by the filled square.

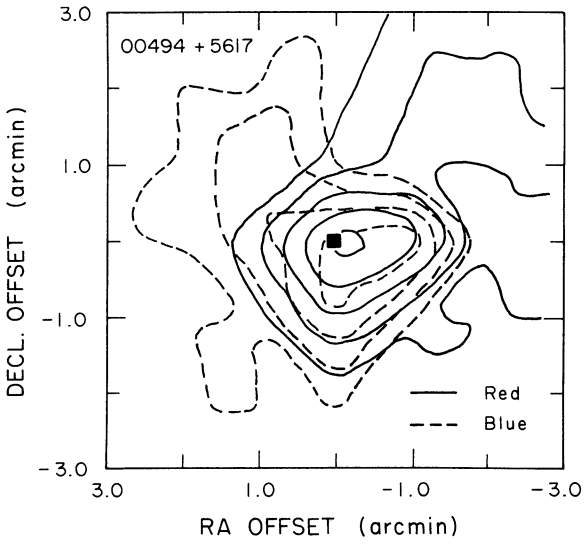

FIG. 7.—Maps of the integrated ^{12}CO intensity of the high-velocity redshifted (-28 to -20 km s^{-1}) and blueshifted (-40 to -34 km s^{-1}) emission near 00494+5617. The location of 00494+5617 is indicated by the filled square.

ii) *00494+5617*

This source lies adjacent to the H II region NGC 281 (S184) at a distance of 2.2 kpc (Georgelin and Georgelin 1976). This region has been mapped in ^{12}CO by Elmegreen and Lada (1978), who find two molecular clouds separated by a channel of ionized gas. The source 00494+5617 is coincident with an H_2O maser found by Elmegreen and Lada which lies in the western cloud near the ionization front at the H II region interface. Elmegreen and Lada speculate that the expanding H II regions could have triggered the gravitational instability that resulted in the formation of 00494+5617. Much of the western cloud has been mapped in the present study and is shown in Figure 1; the abrupt decrease in emission north of the source marks the interface with NGC 281.

^{12}CO spectra directly toward 00494+5617 and to the east and west are shown in Figure 6. The line width toward the source is considerably greater than is seen in the off-source spectra, the full extent of the line toward the source being 16 km s^{-1}. A map of the integrated intensity in the blue (-40 to -34 km s^{-1}) and red (-28 to -20 km s^{-1}) line wings is presented in Figure 7. The maximum integrated intensity in both wings is found toward 00494+5617, and there is little other evidence that the outflow is bipolar. The high-velocity emission is largely restricted to a region about 2′ (1.3 pc) in diameter and centered on the infrared source.

iii) *05358+3543*

The source 05358+3543 lies toward the H II region S233, which is approximately 25′ west and 5′ south of S235. The latter object is estimated to lie at a distance of 1.8 kpc (Evans and Blair 1981). The CO emission near S235 has been mapped by Evans and Blair (1981), who found velocity components at -17 and -20 km s^{-1}, but their map did not extend to the west far enough to overlap 05358+3543. A spectrum toward 05358+3543 is shown in Figure 8; weak but extended wings

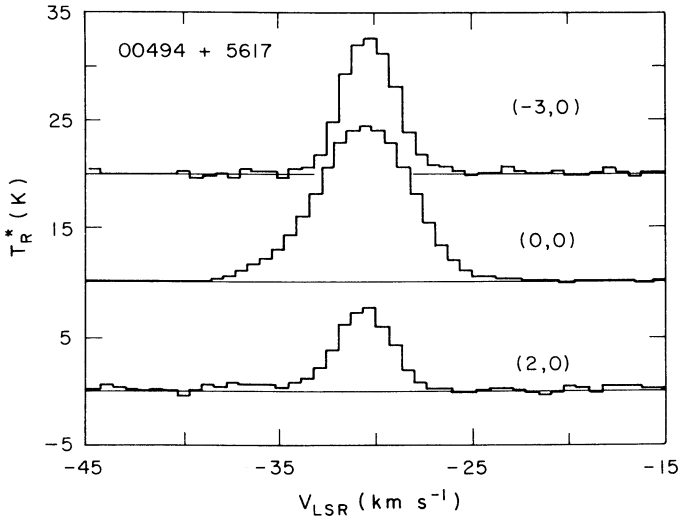

FIG. 6.—Spectra of the ^{12}CO line obtained 3′ west, toward, and 2′ east of 00494+5617.

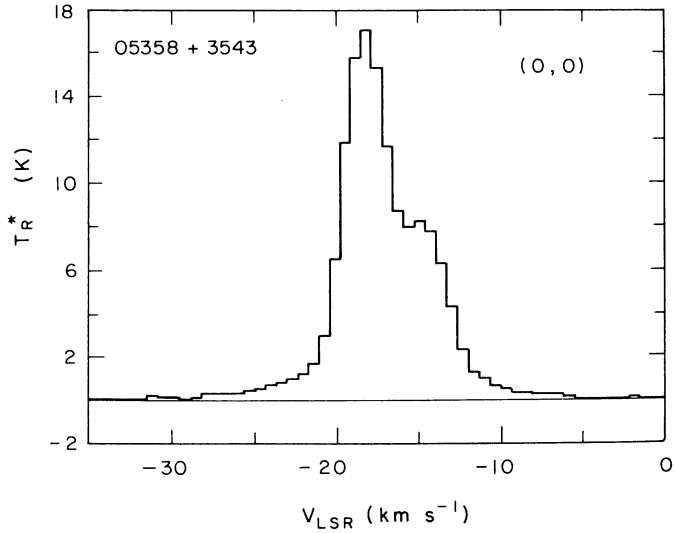

FIG. 8.—^{12}CO spectrum obtained toward 05358+3543

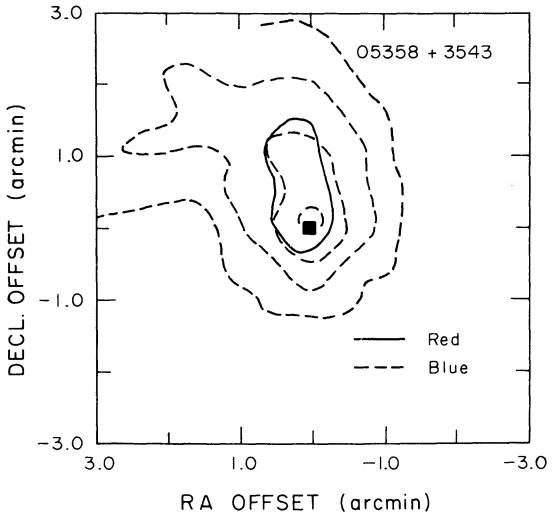

FIG. 9.—Maps of the integrated ^{12}CO intensity of the high-velocity redshifted (−12 to −6 km s^{-1}) and blueshifted (−30 to −21 km s^{-1}) emission near 05358 + 3543. The location of 05358 + 3543 is indicated by a filled square.

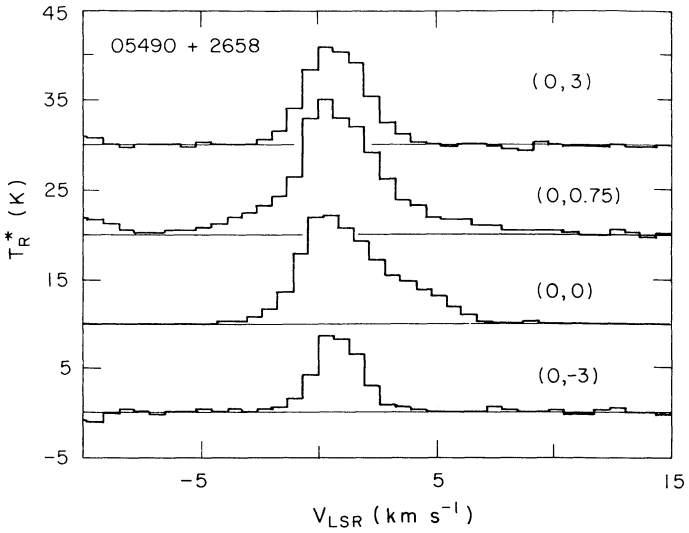

FIG. 10.—^{12}CO spectra obtained in four locations near 05490 + 2658. The locations from top to bottom are 3′ north, 0.′75 north, toward, and 3′ south of 05490 + 2658.

can be seen, with a total velocity extent of 25 km s^{-1}. The extent of the very high velocity gas is poorly determined, since the mapping data did not generally have the same sensitivity as the spectrum shown in Figure 8. A map of the integrated intensity of the blueshifted (−30 to −21 km s^{-1}) and redshifted (−12 to −6 km s^{-1}) emission is shown in Figure 9. Emission in both wings peaks at the position of 05358 + 3543 and shows no evidence for bipolar structure. The emission is extended over a region several arcminutes (1 pc) in size.

iv) *05490 + 2658*

This source lies roughly 5′ east of the H II region S242, estimated to be at a distance of 2.1 kpc (estimated by Y. Georgelin and quoted by Blitz, Fich, and Stark 1982), and the velocity of the CO emission seen is the same as that found toward S242 (Blitz, Fich, and Stark 1982). The source 05490 + 2658 also lies close to the supernova remnant Simeis 147 (see Huang and Thaddeus 1986). Spectra toward 05490 + 2658 and to the north and south are shown in Figure 10; pronounced redshifted emission and weak blueshifted emission are seen directly toward the source, but more striking red and blue wings are seen in the spectra obtained 0.′75 north of the source. A map of the integrated intensity in the blue (−8 to −2 km s^{-1}) and red (5 to 12 km s^{-1}) wings is presented in Figure 11. The strongest emission in both wings is found about 1′ northwest of 05490 + 2658, where the total velocity extent is 20 km s^{-1}. The displacement of 05490 + 2658 from the center of the molecular outflow may be barely within the typical positional uncertainty claimed for the *IRAS* point sources and thus cannot be judged to be significant. The emission is extended over 1.′5 (0.9 pc) and shows no evidence for a bipolar morphology.

v) *05553 + 1631*

This source lies 1.′5 south and 3° west of S254–S258 and has approximately the same radial velocity as the clouds associated with this complex of H II regions (Evans, Blair, and Beckwith 1977). The distance of S254–S258 has been estimated to be 2.5 kpc (Moffat, FitzGerald, and Jackson 1979, hereafter MFJ). The clouds in this region make up a large cloud complex mapped by Huang and Thaddeus (1986), and at the northern end of the complex lie S252 and the Gem OB1 association, estimated to be at a distance of 1.5 kpc (Humphreys 1978). The emission associated with S252 and that associated with S255–S258 have the same radial velocity. Thus, it is not clear whether S252 and S255–258 comprise one large cloud and the distance to one of these sources is in error, or whether there are two separate clouds aligned along the line of sight. We adopt a distance of 2.5 kpc for 05553 + 1631.

Spectra obtained in the vicinity of 05553 + 1631 are shown in Figure 12. The spectrum toward the source is symmetrical in shape, with extended red and blue wings. The spectrum taken 0.′75 east shows a pronounced blue wing, while the spectrum taken 0.′75 south and 0.′75 west shows a pronounced red wing. The spectrum toward 05553 + 1631 has full velocity extent of 17 km s^{-1}. A map of the integrated intensity in the blue (−3 to 4 km s^{-1}) and red (7 to 14 km s^{-1}) wings is presented in Figure 13. The red and blue wings define a striking bipolar outflow

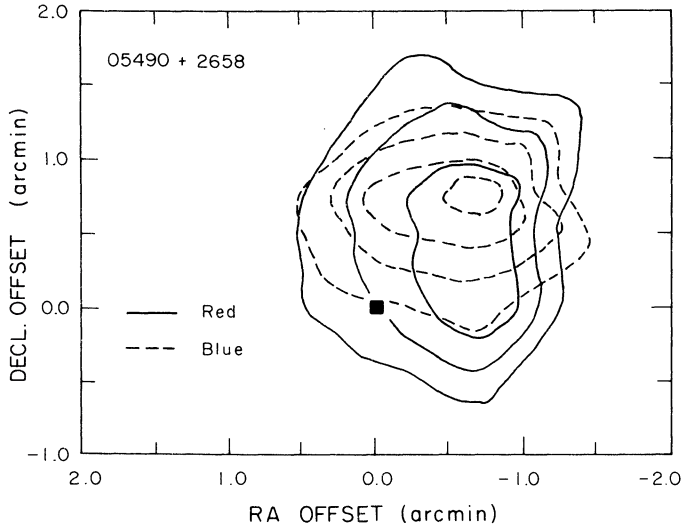

FIG. 11.—Maps of the integrated ^{12}CO intensity of the high-velocity redshifted (5 to 12 km s^{-1}) and blueshifted (−8 to −2 km s^{-1}) emission near 05490 + 2658. The location of 05490 + 2658 is indicated by the filled square.

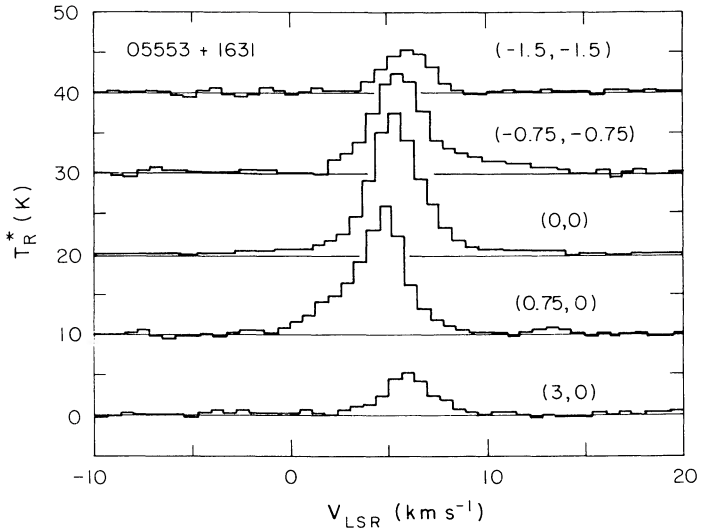

FIG. 12.—Spectra of the ^{12}CO line near 05553 + 1631. The spectra from top to bottom were obtained at locations 1.'5 west and 1.'5 south, 0.'75 west and 0.'75 south, toward, 0.'75 east, and 3′ east of 05553 + 1631.

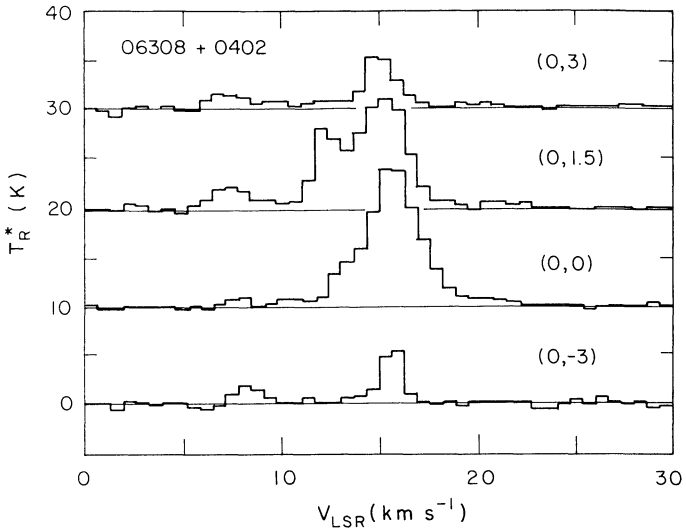

FIG. 14.—^{12}CO spectra obtained in four locations near 06308 + 0402. From top to bottom the position at which these spectra were obtained are 3′ north, 1.5′ north, toward, and 3′ south of 06308 + 0402.

with 05553 + 1631 lying near the symmetry axis of the outflow. The full spatial extent of the outflow is roughly 4′ (3 pc).

vi) *06308 + 0402*

The source 06308 + 0402 lies 1° southeast of the Rosette Nebula in the Mon OB2 molecular cloud. This region has been mapped by Blitz and Thaddeus (1980), and they find the CO emission to be peaked toward the infrared source GL 961. The small map of the 06308 + 0402 region shown in Figure 1 shows this source to be associated with a secondary peak in the CO emission in this region, roughly 20′ southwest of GL 490 but not discernible on the low-resolution maps of Blitz and Thaddeus (1980). The distance to this region has been estimated by Blitz and Thaddeus to be 1.6 kpc. This source also lies toward a cluster of red nebulous stars, RNO 73 (Cohen 1980).

Spectra obtained in the vicinity of 06308 + 0402 are shown in Figure 14. The spectral lines 3′ north and south of 06308 + 0402 are very narrow; a weak secondary velocity feature is also present at a velocity of 8 km s^{-1}. Toward the *IRAS* source the line is much broader, with a full velocity extent of 12 km s^{-1}. In the spectrum obtained 1.'5 north of the source the line splits into two components at 15 and 12 km s^{-1}; the relation of the 12 km s^{-1} component to the outflow is unclear. A map of the integrated intensity of the blue (10–14 km s^{-1}) and red (17–22 km s^{-1}) line wings is shown in Figure 15. The red wing is centered on 06308 + 0402, but the peak in the blue wing is located north of the source, where the 12 km s^{-1} feature is the strongest. The spatial extent of the 12 km s^{-1} feature is small and localized near the infrared source. We tentatively identify this feature as emission from the molecular gas swept up by the stellar wind from 06308 + 0402. The relatively low radial velocities of the molecular outflow in this source and the peculiar line profiles make the identification of this region as an outflow less certain than the five objects discussed earlier.

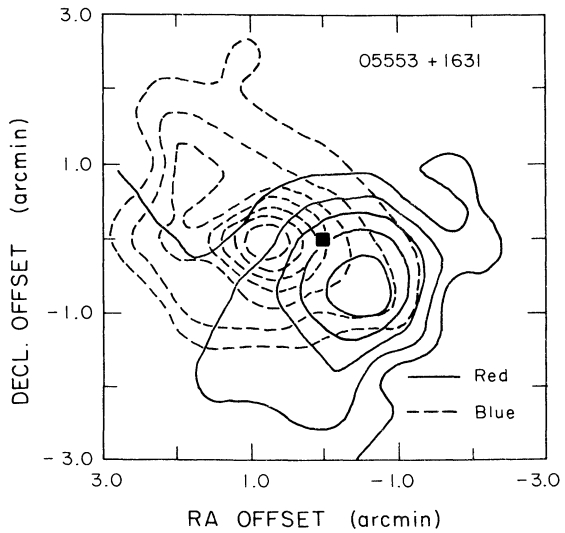

FIG. 13.—Maps of the integrated ^{12}CO intensity of the high-velocity redshifted (7 to 14 km s^{-1}) and blueshifted (−3 to 4 km s^{-1}) emission near 05553 + 1631. The location of 05553 + 1631 is indicated by a filled square.

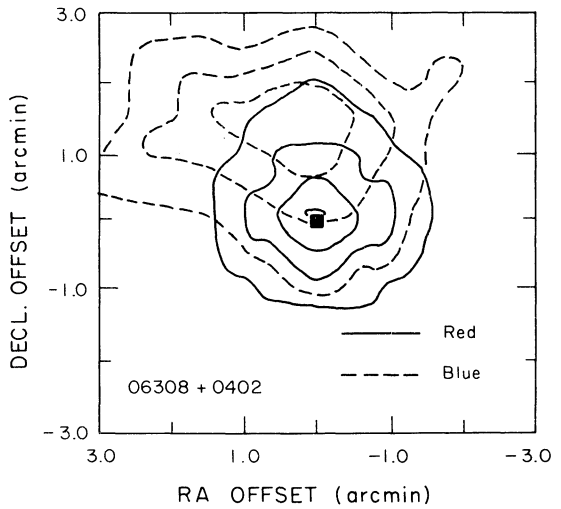

FIG. 15.—Maps of the integrated ^{12}CO intensity of the high-velocity redshifted (17 to 22 km s^{-1}) and blueshifted (10 to 14 km s^{-1}) emission near 06308 + 0402. The location of 06308 + 0402 is indicated by the filled square.

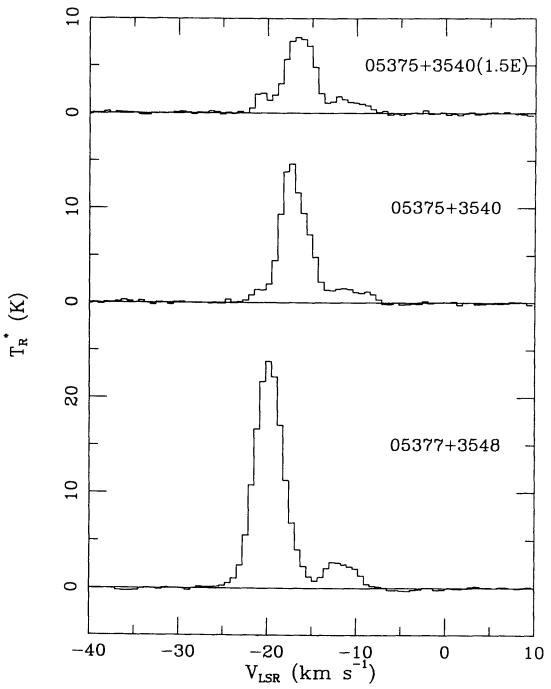

FIG. 16.—^{12}CO spectra obtained toward 05375+3540 (*middle spectrum*), 1'.5 east of 05375+3540 (*upper spectrum*), and toward 05377+3548 (*lower spectrum*).

vii) *05375+3540 (S235B)*

This source is identified as an outflow by Lada (1985) on the basis of a single spectrum obtained by Bally and Lada (1983). The velocity width of the ^{12}CO emission at 0.1 K was measured by Bally and Lada to be 22 km s^{-1}, and we find similar line widths in our measurements. A spectrum obtained toward this source is shown in the middle panel of Figure 16. However, the large width of the CO line is due primarily to the blending of three velocity components, one narrow and strong feature at -17 km s^{-1}, a weaker and broader component centered at -11 km s^{-1}, and another weak feature at a velocity of -20 km s^{-1}. A 3 × 3 point map spaced by 1'.5 showed that these three features persist over the entire map and that the weak blue feature seen toward 05375+3540 is indeed a third velocity component at -21 km s^{-1} (see the top spectrum in Fig. 16 obtained pointing 1'.5 east of 05375+3540). All three components are also seen in the mapping data obtained around 05377+3548, located approximately 8' north of 05375+3540. Toward 05377+3548 (lower spectrum in Fig. 16), the -20 km s^{-1} feature is the strongest velocity component in the spectrum and is blended with the -17 km s^{-1} component; the -11 km s^{-1} feature is stronger toward 05377+3548 than toward 05375+3540. In addition, all three velocity components are detected and discussed by Evans and Blair (1981). Thus, we conclude that the large width of the CO emission seen in this region is due to a superposition of velocity components and is not obviously due to the presence of a molecular outflow. This region illustrates that line widths and shapes can be misleading and that without mapping data the identification of outflows can be difficult.

b) Outflow Energetics

We have computed the mass, momentum, and energy of the molecular outflows using the techniques discussed in Paper I. We summarize these here. In computing the total gas column densities, we assume that the high-velocity ^{12}CO emission is optically thin, that the populations of the various rotational levels are in LTE at a gas kinetic temperature of 25 K, and that the ratio CO/H_2 is 10^{-4}. It should be noted that Snell *et al.* (1984) and Margulis and Lada (1985) have measured the ^{13}CO emission from a small sample of molecular outflows and found that high-velocity ^{12}CO emission is often optically thick. Thus, the column densities in the outflows can be underestimated if saturation is not taken into account. However, without ^{13}CO observations it is not possible to determine the optical depth of the high-velocity ^{12}CO emission, and thus it is not possible to correct for this effect. Consequently, the quoted masses, momenta, and energies are likely to be lower limits to their true values.

A minimum value for the mass of high-velocity gas can be computed by summing up the contributions to the mass at each location in the outflow using the above technique; these results are summarized in Table 3. Momenta and energies have been estimated by computing the integrals

$$\int T_R\,|v - v_0|\,dv\,, \qquad \int T_R(v - v_0)^2\,dv$$

over the velocity range of the high-velocity emission, where v_0 is the velocity of the ambient cloud (see Paper I). The total momentum and energy in the outflows are then determined by

TABLE 3

PROPERTIES OF OUTFLOWS

Source	Mass ($M_\odot$)	Momentum ($M_\odot$ km s^{-1})	Energy (ergs)	Age (yr)	Force ($M_\odot$ km s^{-1} yr^{-1})	Luminosity ($L_\odot$)
00338+6312	2.5	13.2	7.9×10^{44}	1.1×10^5	1.2×10^{-4}	0.06
00494+5617	11.4	59.2	3.4×10^{45}	2.4×10^5	2.5×10^{-4}	0.12
02575+6017[a]	9.7	33.1	1.2×10^{45}	1.7×10^5	1.9×10^{-4}	0.06
05274+3345[a]	4.9	14.3	6.0×10^{44}	2.0×10^5	7.2×10^{-5}	0.03
05345+3157[a]	7.6	37.1	2.0×10^{45}	1.9×10^5	2.0×10^{-4}	0.09
05358+3543	15.7	87.8	5.4×10^{45}	1.7×10^5	5.2×10^{-4}	0.26
05490+2658	7.1	25.5	9.7×10^{44}	3.7×10^5	6.9×10^{-5}	0.02
05553+1631	11.9	44.3	2.0×10^{45}	4.6×10^5	9.6×10^{-5}	0.04
06056+2131[a]	3.4	20.1	1.3×10^{45}	1.1×10^5	1.8×10^{-4}	0.10
06058+2138[a]	2.3	12.7	7.6×10^{44}	6.8×10^4	1.9×10^{-4}	0.09
06308+0402	7.0	36.9	1.4×10^{45}	1.6×10^5	2.3×10^{-4}	0.07
Average	7.6	34.9	1.8×10^{45}	2.0×10^5	1.9×10^{-4}	0.09
σ	4.1	21.7	1.4×10^{45}	1.1×10^5	1.2×10^{-4}	0.06

[a] From Paper I.

converting the integrated intensities to column densities and summing the contributions from all parts of the outflows. Estimates of the momenta and energies are presented in Table 3. We can also estimate a dynamical time scale or "age" for the outflows by simply dividing their transverse sizes by their average velocities. These time scales are almost certainly *overestimates*, since we have used the mass-weighted velocities, which are several times smaller than the maximum outflow velocity observed. Finally, we have computed the force and the mechanical luminosity of each outflow. These measure the rate of deposition of momentum and energy to the molecular gas. The age, force, and mechanical luminosity are presented for each source in Table 3. The properties of the outflows studied in Paper I are also summarized in Table 3 and are similar to the properties of the six outflows presented here.

The outflows found in this survey and in Paper I represent a very homogeneous sample, with the range in physical properties varying by only a factor of a few from their average. The properties of these outflows can be compared with several well-studied outflows that also satisfy our selection criteria; these are AFGL 490, NGC 2071, and NGC 2264 (Snell *et al.* 1984; Margulis, Lada, and Snell 1988). Two striking differences are found between these three outflows and those in our sample: the three outflows have significantly higher velocities and smaller ages. As pointed out in Paper I, the smaller velocities found for outflows in our survey as compared with the previously detected outflows are likely a selection effect in which the outflows with the most prominent line wings were the first to be identified. It is also possible that the differences in age may be related to the differences in velocity, since it is expected that the velocity of the molecular gas would decrease with time as more and more material is accumulated in the swept-up molecular shell. In fact, the molecular shell would decelerate even more rapidly once the stellar winds begin to diminish in strength.

In general, it is not possible to determine whether the stellar winds are still active in these embedded sources. Therefore, it is possible that the lifetime of the stellar wind is significantly shorter than the dynamical age of the molecular outflows and that the molecular outflows in our sample may not be currently driven by a stellar wind but may be only coasting. A shorter stellar wind lifetime would have important consequences in computing the stellar wind energetics. For instance, since the force presented in Table 3 is averaged over the dynamical age of the outflow, if the stellar wind accelerated the gas over a much shorter time, the force in the wind would have to be much larger. If the interaction between the stellar wind and the molecular shell is momentum-conserving and if the winds are active over the dynamical age of the outflow, then the force provided by radiation pressure is nearly sufficient to power the winds in all of the sources. However, if the stellar winds blow for only a small fraction of the dynamical age of the molecular outflow, then radiation pressure is insufficient to drive the wind.

If we assume momentum conservation, a stellar wind velocity of 200 km s^{-1}, and a stellar wind that is active over the dynamical age of the molecular outflow, we can estimate the stellar wind energetics. The mechanical luminosity of the wind can be estimated from $L_w = L_{out} \times V_w/V_{out}$, where the subscript "out" denotes the outflow and w the stellar wind, and the stellar wind luminosity has been found to range from 1.1 to 9.3 $L_\odot$, with an average value of 3.5 $L_\odot$. The wind luminosity is on average about 0.07% of the radiant luminosity of the stellar sources (the range for the outflows in our sample is from 0.03% to 0.15%). We can also estimate the mass-loss rate in the stellar wind from $dM_w/dt = F_{out}/v_w$, where F is the average force in the molecular outflow and v_w is the stellar wind velocity. The average mass-loss rate is 10^{-6} $M_\odot$ yr^{-1}, and the range is from 3.5×10^{-7} to 2.6×10^{-6} $M_\odot$ yr^{-1} for the 11 outflows. If the lifetime of the stellar wind is 10 times shorter than the dynamical age of the outflow (approximately 2×10^4 yr), than the stellar wind luminosity and mass-loss rate would be 10 times larger.

IV. DISCUSSION

The primary goal of this study was to improve the statistics on the occurrence of molecular outflows associated with bright and, as we have shown, luminous infrared sources. We have detected six new outflows among a sample of 21 objects investigated in this study, and in Paper I we detected five new outflows in a sample of 18. Also meeting our criteria were 11 previously detected outflows (Lada 1985), S187, W3, W3OH, AFGL 437, AFGL 490, HH 12, LkHα 101, NGC 2071, S255, AFGL 961, and NGC 2264, all of which would have been readily detected with the sensitivity and search techniques used in this study. Thus, out of a sample of 51 objects meeting our selection criteria, 22 have associated molecular outflows. We thus confirm the high detection rate (roughly 0.5) of outflows associated with luminous infrared sources reported in Paper I.

Our new observations support the claim made in Paper I that the duration of young stellar objects as bright far-infrared sources must be less than about 4×10^5 yr (i.e., roughly twice the outflow lifetime), since, if the lifetimes of YSOs as far-infrared sources were much longer than 4×10^5 yr, we should have detected a much larger number of sources *without* outflows. As a consequence of this fact, the time scale to disrupt the dense envelopes of gas and dust that veil luminous young stars must be fairly short. Since the time frame in which YSOs are bright far-infrared sources appears to coincide closely with the outflow stage, it is likely that outflows are the main agent responsible for unveiling dust-enshrouded young stars.

We can also examine the occurrence of outflows in our sample as a function of infrared color and luminosity. In the color-color and color-luminosity diagrams shown in Figures 2 and 3, the sources with outflows and without outflows are indicated. As can be seen, there is no difference between the positions of outflow and nonoutflow sources in these diagrams. Thus, there is no obvious physical difference in sources with and without outflows. The lack of any evolutionary trends may be a consequence of our selection criteria; by choosing bright far-infrared sources, we may have inadvertently selected objects at a similar evolutionary stage.

The clouds associated with 21 of the far-infrared sources in our sample were mapped in ^{12}CO and ^{13}CO by Carpenter, Snell, and Schloerb (1989); they found that on average each far-infrared source was associated with approximately 5×10^3 $M_\odot$ of cloud material. Accounting for the 50% detection rate of this survey, there is approximately 1×10^4 $M_\odot$ of cloud material per detected outflow, slightly higher than the 3×10^3 $M_\odot$ per outflow found in the Orion and Mon OB1 outflow surveys (Fukui *et al.* 1986; Margulis, Lada, and Snell 1988). This difference may be in part due to the greater distance of the sources in our sample relative to Orion and Mon OB1. Thus, we may have missed many of the lower-energy outflows in these regions; in addition, we have not surveyed the entire 5×10^3 $M_\odot$ of material for outflows.

The total momentum and energy contained within the outflows detected in this work are quite significant and may have a major impact on the energy balance of the surrounding clouds. Our estimate of the average momentum and kinetic energy in these outflows is 34.9 $M_\odot$ km s^{-1} and 2×10^{45} ergs, respectively, but these estimates do not include corrections for optical depth effects in the mass determination or for inclination effects in the velocity determinations. Therefore, the momenta and energies are likely to be significantly larger than those quoted in Table 3. Corrections for these two effects (Snell 1987) can easily increase the average momentum in an outflow by a factor of 5 and the average energy by a factor of 10. A better estimate of the mean outflow energy of the sources studied in this work is therefore 2×10^{46} ergs.

We can estimate how important outflows are to the overall energy budget within clouds by balancing the energy input rate through outflows against the energy dissipation rate in clouds. The energy input rate into the clouds via outflows is roughly given by

$$L_{\rm in} \approx f\eta E_{\rm out}/\tau_{\rm out} ,$$

where $E_{\rm out}$ is the typical energy of an outflow, f the fraction of time over which the outflow is "on," η the efficiency with which the outflow energy is distributed over the cloud mass, and $\tau_{\rm out}$ the outflow lifetime. Substituting the average outflow energy and lifetime estimated above, we find $L_{\rm in} = 0.8 f\eta\ L_\odot$. In comparison, the kinetic energy in clouds is roughly $3M\sigma^2/2$, where M is the mass of the cloud and σ the one-dimensional velocity dispersion, and the dissipation time scale can be roughly approximated by the crossing time $\mathscr{L}/\sigma$, where $\mathscr{L}$ is the cloud size. Thus, the energy dissipation rate is given roughly by

$$L_{\rm out} \approx 3\ M\sigma^3/2\mathscr{L} .$$

Using masses of $5 \times 10^3\ M_\odot$, one-dimensional velocity dispersions of 2 km s^{-1} (corresponding to $\Delta v_{\rm FWHM} = 5$ km s^{-1}), and cloud sizes of 5 pc, measured by Carpenter, Snell, and Schloerb (1989), gives $L_{\rm out} = 2.1\ L_\odot$. Since we directly observe the energy in the swept-up ambient molecular gas, the value of η is unity, and we have already estimated f to be approximately 0.5. Thus, outflows may be an important source of kinetic energy in molecular clouds. It is worth noting that since the dynamical ages of the outflows are almost certainly too large, the energy input rate may be considerably higher.

In summary, we have found that (1) virtually all of the *IRAS* sources with 100 μm flux densities greater than 500 Jy are luminous YSOs, (2) roughly one-half of these bright far-infrared sources have associated molecular outflows and the outflow phase must begin shortly after stars begin to produce significant radiant luminosity, (3) the lifetime of these luminous far-infrared sources is at most 4×10^5 yr, with the outflows probably playing a major role in disrupting the dense envelope of gas surrounding the stars, and (4) the outflows associated with luminous YSOs are very energetic and make a significant contribution to the kinetic energy density within molecular clouds.

This work was supported in part by NSF grant AST 85-12903 to the Five College Radio Astronomy Observatory.

REFERENCES

Bally, J., and Lada, C. J. 1983, *Ap. J.*, **265**, 824.
Blitz, L., Fich, M., and Stark, A. 1982, *Ap. J. Suppl.*, **49**, 183.
Blitz, L., and Thaddeus, P. 1980, *Ap. J.*, **241**, 676.
Carpenter, J., Snell, R. L., and Schloerb, F. P. 1989, in preparation.
Casoli, F., Dupraz, C., Gerin, M., Combes, F., and Boulanger, F. 1986, *Astr. Ap.*, **169**, 281.
Cohen, M. 1980, *A.J.*, **85**, 29.
Cohen, R. S., Cong, H., Dame, T. M., and Thaddeus, P. 1980, *Ap. J. (Letters)*, **239**, L53.
Crampton, D., Georgelin, Y. M., and Georgelin, Y. P. 1978, *Astr. Ap.*, **66**, 1.
Dame, T. M., *et al.* 1987, *Ap. J.*, **322**, 706.
Elmegreen, B. G., and Lada, C. J. 1978, *Ap. J.*, **219**, 467.
Evans, N. J., II, and Blair, G. N. 1981, *Ap. J.*, **249**, 394.
Evans, N. J., II, Blair, G. N., and Beckwith, S. 1977, *Ap. J.*, **217**, 448.
Fich, M., and Blitz, L. 1984, *Ap. J.*, **279**, 125.
Fukui, Y., Sugitani, K., Takaba, H., Iwata, T., Mizuno, A., Ogawa, H., and Kawabata, K. 1986, *Ap. J. (Letters)*, **311**, 85.
Georgelin, Y. M., and Georgelin, Y. P. 1976, *Astr. Ap.*, **49**, 57.
Huang, Y.-L., and Thaddeus, P. 1986, *Ap. J.*, **309**, 804.
Humphreys, R. M. 1978, *Ap. J. Suppl.*, **38**, 309.
IRAS Point Source Catalog. 1985, Joint *IRAS* Science Working Group (Washington, DC: GPO).
Lada, C. J. 1985, *Ann. Rev. Astr. Ap.*, **23**, 267.
Margulis, M., and Lada, C. J. 1985, *Ap. J.*, **299**, 925.
———. 1986, *Ap. J. (Letters)*, **309**, L87.
Margulis, M., Lada, C. J., and Snell, R. L. 1988, *Ap. J.*, **333**, 316.
Moffat, A. F. J., FitzGerald, M. P., and Jackson, P. D. 1979, *Astr. Ap. Suppl.*, **38**, 197.
Price, S. D. 1977, *The AFGL Four Color Sky Survey: Supplemental Catalog*, (AFGL-TR-77-0160).
Price, S. D., and Walker, R. G. 1976, *The AFGL Four Color Sky Survey: Catalog of Observations at* 4.2, 11.0, 19.8, *and* 27.4 μm (AFGL-TR-76-0208).
Snell, R. L. 1987, in *IAU Symposium 115, Star Forming Regions*, ed. M. Peimbert and J. Jugaku (Dordrecht: Reidel), p. 213.
Snell, R. L., Huang, Y.-L., Dickman, R. L., and Claussen, M. J. 1988, *Ap. J.*, **325**, 853 (Paper I).
Snell, R. L., Scoville, N. Z., Sanders, D. B., and Erickson, N. R. 1984, *Ap. J.*, **284**, 176.
Turner, D. G. 1976, *Ap. J.*, **210**, 65.
Wood, D. S. O., and Churchwell, E. 1989, *Ap. J.*, **340**, 265.

R. L. DICKMAN and R. L. SNELL: Five College Radio Astronomy Observatory, Lederle Graduate Research Center, University of Massachusetts, Amherst, MA 01003

Y.-L. HUANG: Institute of History, Tsing-Hua University, Hsin-Chu, Taiwan, Republic of China